Dynamical Forcing of Subseasonal Variability in the Tropical Brewer–Dobson Circulation

MARTA ABALOS*

Universidad Complutense de Madrid, Madrid, Spain

WILLIAM J. RANDEL

National Center for Atmospheric Research,+ Boulder, Colorado

ENCARNA SERRANO

Universidad Complutense de Madrid, Madrid, Spain

(Manuscript received 15 November 2013, in final form 16 April 2014)

ABSTRACT

Upwelling across the tropical tropopause exhibits strong subseasonal variability superimposed on the well-known annual cycle, and these variations directly affect temperature and tracers in the tropical lower stratosphere. In this work, the dynamical forcing of tropical upwelling on subseasonal time scales is investigated using the European Centre for Medium-Range Weather Forecasts (ECMWF) Interim Re-Analysis (ERA-Interim) for 1979–2011. Momentum balance diagnostics reveal that transience in lower-stratospheric upwelling is linked to the effects of extratropical wave forcing, with centers of action in the extratropical winter stratosphere and in the subtropical upper troposphere of both hemispheres. The time-dependent forcing in these regions induces a remote coupled response in the zonal mean wind and the meridional circulation (with associated temperature changes), which drives upwelling variability in the tropical stratosphere. This behavior is observed in the reanalysis, consistent with theory. Dynamical patterns reflect distinctive forcing of the shallow versus deep branches of the Brewer–Dobson circulation; the shallow branch is most strongly correlated with wave forcing in the subtropical upper troposphere and lower stratosphere, while the deep branch is mainly influenced by high-latitude planetary waves.

1. Introduction

Tropical upwelling is an important component of the Brewer–Dobson circulation (BDC), strongly influencing temperature and tracer distributions in the tropical lower stratosphere (e.g., Holton et al. 1995; Plumb 2002; Shepherd 2007). The tropical BDC is mainly driven by momentum deposition from large- and small-scale waves, but the relative roles of different forcing regions and their contributions for variability on different time scales are topics of ongoing research (e.g., Randel et al. 2008; Taguchi 2009; Ueyama and Wallace 2010; Zhou et al. 2012; Ueyama et al. 2013). There is empirical evidence that wave activity in the extratropical winter stratosphere influences upwelling and temperatures in the tropical lower stratosphere (e.g., Fritz and Soules 1972; Randel 1993; Randel et al. 2002; Ueyama and Wallace 2010). This influence occurs as the extratropical waves exert a drag on the zonal mean circulation, inducing poleward mass flow, with mass continuity requiring downward flux at high latitudes and upwelling at low latitudes (e.g., Andrews et al. 1987). Theoretical considerations imply that, in the steady-state limit, these induced vertical motions are limited to the latitudinal extent of the forcing (cf. the ''downward control principle''; Haynes et al. 1991), and this suggests that wave forcing needs to occur close to the tropics in order to produce realistic mean tropical upwelling (Plumb and Eluszkiewicz 1999;

* Current affiliation: Laboratoire de Météorologie Dynamique (CNRS), Paris, France.

+ The National Center for Atmospheric Research is sponsored by the National Science Foundation.

Corresponding author address: Marta Abalos, Depto. Geofísica y Meteorología, Universidad Complutense de Madrid, Facultad de CC. Físicas, Avda. Complutense s/n, 28040 Madrid, Spain.
E-mail: mabalosa@ucm.es

DOI: 10.1175/JAS-D-13-0366.1

Semeniuk and Shepherd 2001). In contrast, for transient conditions, the influence of extratropical wave forcing can extend into the tropics through nonlocal effects (Garcia 1987; Haynes et al. 1991). The remote connection between high and low latitudes results from the coupled response of the atmospheric zonal wind, temperature, and meridional circulation to a transient wave drag (Garcia 1987).

There has been substantial interest in understanding the forcing responsible for the relatively large annual cycle in tropical upwelling, which in turn mainly drives the seasonality in temperature and chemical tracers in the tropical lower stratosphere (e.g., Yulaeva et al. 1994; Randel et al. 2007; Abalos et al. 2012, 2013). However, causality is difficult to untangle for the annual cycle, and the roles of different regions and types of wave forcing have been emphasized in a number of studies (including forcing from high latitudes, subtropics, and tropics). Based on the observed coherent temperature annual variations in the tropics and extratropics, some analyses have proposed a primary role of extratropical planetary waves (Yulaeva et al. 1994; Ueyama and Wallace 2010). However, as noted above, strictly high-latitude forcing is difficult to reconcile with theoretical expectations for time-mean tropical upwelling. Ueyama et al. (2013) recently suggested that the influence of the extratropical wave drag may involve the latitudinal progression of the forcing toward the tropics on time scales of about 10 days. Wave driving in the subtropics resulting from the dissipation of midlatitude baroclinic eddies has been emphasized by Taguchi (2009) and Chen and Sun (2011). Furthermore, several studies have highlighted an important role of equatorial planetary waves forced by convection in driving the seasonality in upwelling around the tropical tropopause (Boehm and Lee 2003; Kerr-Munslow and Norton 2006; Ryu and Lee 2010; Ortland and Alexander 2014). Randel et al. (2008) noted strong seasonal variations for wave forcing in the subtropics, resulting from the combined effects of extratropical and equatorial wave fluxes. The importance of subtropical wave drag has been also noticed in relation to the long-term trends in upwelling predicted by models (Butchart et al. 2006; Garcia and Randel 2008; Calvo and Garcia 2009; Garny et al. 2011; Shepherd and McLandress 2011).

Observations suggest large variability in tropical upwelling on subseasonal time scales. Although the theory of transient driving of the meridional circulation is well understood, observations of the dynamical forcing mechanisms for subseasonal fluctuations in upwelling have been less well documented. The relation between transience in the tropical lower stratosphere and sporadic bursts of planetary wave activity in the stratospheric high latitudes has been assessed in some observational works (e.g., Yulaeva et al. 1994; Randel et al. 2002; Ueyama and Wallace 2010). Zhou et al. (2012) argued that extratropical and subtropical wave drag act cooperatively to drive upwelling on various time scales and highlighted the importance of including transient variability for determining the specific forcing latitudes. Using high-vertical-resolution GPS temperature measurements, Grise and Thompson (2013) analyzed the role of different forcing regions in driving transient variability in upwelling (inferred from temperature tendencies). They found that planetary waves in the extratropical and subtropical stratosphere mainly drive transient upwelling in the lower stratosphere (above about 70 hPa), while equatorial planetary waves and drag in the subtropical troposphere are important for upwelling around the tropopause.

In this work, the dynamical drivers of transient variability in upwelling are investigated using daily time series of tropical mean upwelling derived from momentum balance calculations based on European Centre for Medium-Range Weather Forecasts (ECMWF) Interim Re-Analysis (ERA-Interim) data. In contrast with the annual cycle, the distinctive signature of subseasonal fluctuations in upwelling allows isolating the specific forcing using linear correlations and regressions. Section 2 describes the data and analyses and illustrates the statistical signature of the response to an extratropical time-dependent wave drag, as observed in the reanalysis. The forcing regions relevant for transient variability of tropical upwelling in the lower stratosphere are identified through regression and composite analyses in sections 3a and 3b, respectively. In addition to the extratropical winter stratosphere, the subtropical upper troposphere is found to play an important role in driving tropical upwelling, and the remote driving of upwelling by wave drag in this region is explored in section 3c. The connection between the different forcing regions is investigated in section 3d. Distinct circulations and forcings associated with the shallow versus deep branches of the tropical Brewer–Dobson circulation are observed in the results, and this is further analyzed in section 3e. Finally, section 4 presents a summary and discussion of the main results in the context of previous works.

2. Data and analyses

Daily mean temperature and three-dimensional wind fields from ERA-Interim are used (Dee et al. 2011), obtained averaging the 6-hourly data, for the period 1979–2011. The data are archived in a 1.5° × 1.5° grid, on 37 pressure levels spanning from 1000 to 1 hPa. To isolate subseasonal variability, a high-pass filter is applied to all the fields, which retains fluctuations on time scales shorter than 90 days. This threshold is chosen to eliminate the influence of the seasonal cycle up to its fourth harmonic.

The analyses are based on the transformed Eulerian mean (TEM) framework, where the governing equations can be written as

$$\mathrm{DF} = \frac{\partial \overline{u}}{\partial t} - \hat{f}\overline{v}^*, \tag{1}$$

$$\frac{\partial \overline{T}}{\partial t} + \overline{v}^* \frac{1}{a}\frac{\partial \overline{T}}{\partial \phi} + \overline{w}^* S = \overline{Q}, \tag{2}$$

$$(a\cos\phi)^{-1}\frac{\partial}{\partial \phi}(\overline{v}^*\cos\phi) + e^{z/H}\frac{\partial}{\partial z}(\overline{w}^* e^{-z/H}) = 0, \tag{3}$$

$$f\frac{\partial \overline{u}}{\partial z} + \frac{R}{aH}\frac{\partial \overline{T}}{\partial \phi} = 0. \tag{4}$$

In these equations $\mathrm{DF} = (e^{z/H}/a\cos\phi)(\nabla \cdot \mathbf{F})$ is the scaled Eliassen–Palm flux divergence, $(\overline{v}^*, \overline{w}^*)$ is the residual-mean meridional circulation, $\hat{f} = f - (1/a\cos\phi)(\partial/\partial\phi)(\overline{u}\cos\phi)$, and $S = HN^2/R$, with N the Brunt–Väisälä frequency. These equations determine the response of the independent variables $\overline{u}$, $\overline{T}$, $\overline{v}^*$, and $\overline{w}^*$ to the imposed external forcings, DF and $\overline{Q}$ (in practice, $\overline{Q}$ in the tropical lower stratosphere can be approximated as a linear damping proportional to temperature, so that the primary forcing of the system is by the term DF). Combining the TEM momentum equation [Eq. (1)] and mass continuity equation [Eq. (3)], an expression can be derived for tropical upwelling (Randel et al. 2002):

$$\langle \overline{w}^*_m \rangle(z) = \frac{-e^{z/H}\cos\phi}{\int_{-\phi_0}^{\phi_0} a\cos\phi\, d\phi}\left\{ \int_z^\infty \frac{e^{-z'/H}}{\hat{f}(\phi, z')}[\mathrm{DF}(\phi, z') - \overline{u}_t(\phi, z')]_{\overline{m}}\, dz' \right\}_{-\phi_0}^{\phi_0}, \tag{5}$$

where $\overline{u}_t$ is the zonal mean wind tendency. This expression gives tropical upwelling at a given level z averaged over a range of latitudes $(-\phi_0, \phi_0)$ as a function of the net forcing integrated over all altitudes above that level and evaluated at the extremes of the latitudinal interval. In this work the focus is on upwelling in the deep tropics, with Eq. (5) evaluated over 18°N–18°S. This latitude band approximately encompasses the region of strongest upwelling. We note that the results are qualitatively similar for upwelling computed from Eq. (5) using a broader latitudinal band (e.g., 30°N–30°S) and also using altitude and time-dependent turnaround latitudes (not shown). Because the zonal mean angular momentum $\overline{m}$ isolines are almost vertical, the integrand in Eq. (5) can be approximately computed on fixed latitudes. Note that the integrand is a function of the wave forcing (DF) minus $\overline{u}_t$. Thus, from the point of view of the diagnostic Eq. (5), the term $\mathrm{DF} - \overline{u}_t$ can be regarded as the net forcing of upwelling, although it is understood that the actual wave forcing (DF) drives a balanced nonlocal circulation that includes the zonal mean wind response $\overline{u}_t$.

As mentioned in the introduction, the zonal mean response of the atmosphere to a momentum forcing (DF) in the extratropical winter stratosphere, given by Eqs. (1)–(4), has been extensively studied in theoretical models (Garcia 1987; Haynes et al. 1991; Plumb and Eluszkiewicz 1999), and its relation to upwelling in the tropics is fairly well understood for transient wave forcing (e.g., for stratospheric sudden warming events; Dunkerton et al. 1981). Figure 1 illustrates this behavior as derived from one-point correlation cross-sections, calculated from ERA-Interim for subseasonal time scales in boreal winter [December–March (DJFM)]. The reference time series for these correlations is −DF [convergence of the Eliassen–Palm (EP) flux] at one point in the extratropical boreal stratosphere (54°N, 20 hPa), representative of a region with climatological EP flux convergence in DJFM, and Fig. 1 shows the correlations with different fields (DF, $\overline{u}_t$, $\mathrm{DF} - \overline{u}_t$, and $\overline{T}_t$). Wave drag at this particular location is associated with vertical wave propagation from the extratropical troposphere into the stratosphere and a broad region of wave dissipation (EP flux convergence) extending throughout the middle and high latitudes (Fig. 1a). The response in the zonal mean wind (Fig. 1b) shows local deceleration of the zonal mean flow and acceleration on the equatorward side of the forcing (and also negative wind tendencies in the SH subtropics). The net forcing (Fig. 1c) has a broader latitudinal extent than the DF forcing alone, extending into the deep tropics. The residual circulation induced by the forcing in Fig. 1a and the associated impact on temperature (Fig. 1d) show a broad region of upwelling and cooling extending to altitudes in the tropical lower stratosphere, along with downwelling and warming on the poleward side of the forcing. Both the upwelling and the temperature response are found to cross the equator and extend into the SH—a feature clearly seen in satellite observations (Fritz and Soules 1972). The change in temperature gradients in the SH is associated with changes in the zonal mean wind, which is observed in Fig. 1b as the

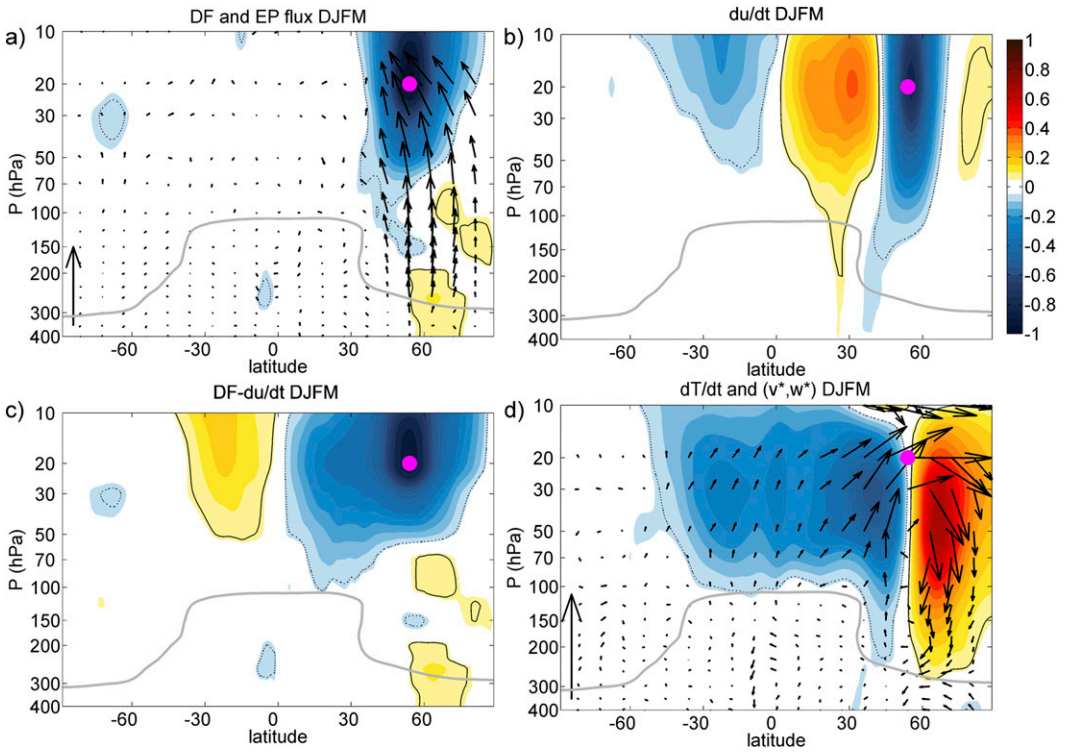

FIG. 1. One-point correlations of EP flux convergence (−DF) at 54°N, 20 hPa with (a) EP flux (vectors) and divergence (colors), (b) zonal mean wind tendency, (c) net forcing, and (d) temperature tendency (colors) and residual circulation (vectors) for DJFM. The solid and dashed contours show the threshold of 99% significant linear correlations (positive and negative, respectively). The seasonal-mean lapse-rate tropopause is shown in gray. The vertical arrows in (a),(d) indicate the length corresponding to a linear correlation of 1 (equal for horizontal and vertical components). All figures are based on ERA-Interim 1979–2011 data unless explicitly stated in the captions.

negative correlations over approximately 10°–40°S. The transient response to localized wave forcing also includes an additional meridional circulation cell of opposite sense above the forcing (Garcia 1987), but this is above the domain shown in Fig. 1.

The statistical relations in Fig. 1 evidence the meridional circulation (Fig. 1d) induced by a localized extratropical forcing (Fig. 1a) in the reanalysis, which is consistent with theoretical models based on the TEM equations [Eqs. (1)–(4)]. In particular, the patterns of correlations in Fig. 1 demonstrate the nonlocal response to high-latitude time-dependent wave forcing, with the residual circulation acting to maintain thermal wind balance between the remotely induced zonal wind and temperature tendencies. A key aspect is that, from a diagnostic point of view, the remote response of $\overline{u}_t$ extends the net forcing toward low latitudes, such that it reaches the boundaries of the tropics [which are most relevant for tropical upwelling; see Eq. (5)]. However, it is important to note that $\overline{u}_t$ should not be interpreted as an additional forcing of upwelling; rather, both $\overline{u}_t$ and the meridional residual circulation constitute two intrinsically linked aspects of the coupled response to localized, transient forcing.

3. Forcing of subseasonal variability in upwelling

The focus of this work is to identify dynamical forcing associated with transient tropical upwelling, and this is done using correlations and regressions applied to $\overline{w}^*_m$. Figure 2a shows daily time series of $\overline{w}^*_m$ at 70 hPa averaged over 18°S–18°N for 2 years (2008/09), illustrating the annual cycle (maximum during boreal winter–spring) together with substantial subseasonal variability. Abalos et al. (2012) showed that these time series of $\overline{w}^*_m$ agree reasonably well (with correlations ~ 0.7) with two other estimates of upwelling (the residual circulation $\overline{w}^*$, derived from ERA-Interim, and a thermodynamic estimate $\overline{w}^*_Q$, based on an accurate radiative transfer code) for the period 2005–10. The thermodynamic estimate is also shown in Fig. 2, highlighting good agreement with $\overline{w}^*_m$. Furthermore, the time series of $\overline{w}^*_m$ are significantly correlated with independent satellite trace-gas observations (ozone and carbon monoxide) on

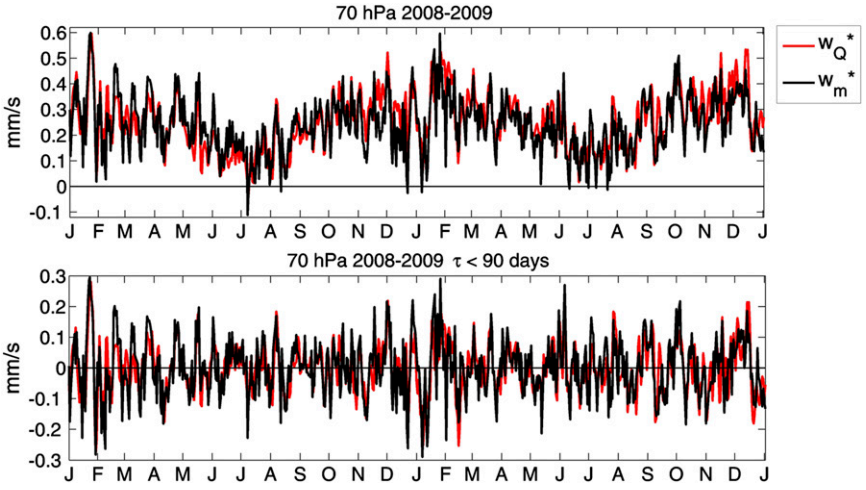

FIG. 2. Time series of upwelling (mm s^{-1}) averaged over 18°S–18°N at 70 hPa for the years 2008/09. Black: momentum balance calculation [Eq. (5)], red: thermodynamic estimate (see text for details). (top) Full time series and (bottom) high-pass-filtered series, including only time scales shorter than 90 days.

subseasonal time scales (Abalos et al. 2012). These results suggest the accuracy of the $\overline{w}^*_m$ estimates and their suitability to investigate the drivers of the variability [i.e., the DF and $\overline{u}_t$ variations that force $\overline{w}^*_m$ via Eq. (5)]. The $\overline{w}^*_m$ time series are filtered to isolate subseasonal time scales as described above, and the filtered data are shown in Fig. 2b; these form the basis of the correlations and regressions described below (based on the full 33-yr record from ERA-Interim); similar results are found for the shorter record 2005–10 used in Abalos et al. (2012) (not shown).

The time series of tropical upwelling at 70 hPa in Fig. 2 are linked to the global zonal mean residual circulation, and Fig. 3 shows the structure of the associated circulations [calculated using ($\overline{v}^*$, $\overline{w}^*$) derived from ERA-Interim] together with the patterns of heating and cooling, for DJFM and June–September (JJAS). In all the latitude–height cross-sections, the regressed zonal mean fields are multiplied by the cosine of latitude to compensate for the increase in variance toward the poles due to spherical geometry (North et al. 1982). In Fig. 3, both seasons show a broad region of tropical upwelling and cooling and high-latitude downwelling and warming in the winter stratosphere. In addition, shallower cells of circulation close to the tropopause are observed linked with warming in the subtropics in both seasons, although the cell on the summer hemisphere is somewhat stronger in DJFM than in JJAS. Below these warming cells there are cooling regions in the subtropical upper troposphere, associated with ascending motion. Enhanced tropical upwelling in the lower stratosphere (70 hPa) is also correlated with warming of the tropical upper troposphere in both seasons. The overall patterns in Fig. 3 are consistent with two branches of the residual circulation, a shallow branch near the tropopause connecting the outer tropics with downwelling over middle latitudes of both hemispheres, and a deep branch that extends from the tropics into the winter polar stratosphere (e.g., Plumb 2002; Birner and Bönisch 2011). The transition between the two branches is further examined in section 3e.

The strong signature of transience in the Brewer–Dobson circulation is also observed in satellite-derived ozone measurements. Figure 4 shows 70-hPa $\overline{w}^*_m$ correlations with zonal mean ozone tendencies ($\partial\overline{O_3}/\partial t$) derived from *Aura* Microwave Limb Sounder (MLS) satellite observations during DJFM and JJAS of the years 2005–10 [as described in Abalos et al. (2012)]. The ozone tendency patterns closely mimic the temperature tendency results (Fig. 3), in particular with patterns in the lower stratosphere that reflect the lower branch of the Brewer–Dobson circulation, and positive correlations in the high-latitude winter stratosphere related to the deep branch. This result reflects the strong influence of vertical circulation anomalies on the region of steep ozone gradients in the lower stratosphere. The coupled ozone–temperature signatures are evidence for coherent variability of the BDC on subseasonal time scales (for both the deep and the shallow branches).

a. Wave drag, wind response, and net forcing

The dynamical driving of transient variability in upwelling in the tropical lower stratosphere is investigated in this section by examining the linear regressions of the different components of the net forcing onto the time series of $\overline{w}^*_m$ at 70 hPa (e.g., Fig. 2b). The regressions for

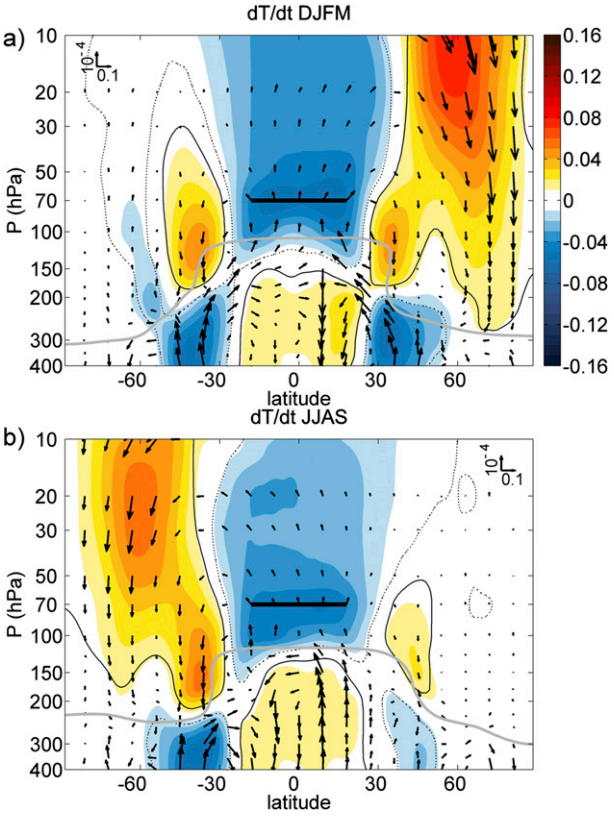

FIG. 3. Regression of the residual circulation (vectors; m s^{-1}) and temperature tendency (colors; K day^{-1}) on tropical upwelling averaged over 18°S–18°N at 70 hPa for (a) DJFM and (b) JJAS. The reference level for upwelling is indicated by the black horizontal bar. The seasonal-mean lapse-rate tropopause is shown in gray. The solid and dashed contours show the threshold of 99% significant linear correlations (positive and negative, respectively). The scale of the vectors is indicated for both vertical and horizontal components. Regression values in all figures are per unit standard deviation in the upwelling.

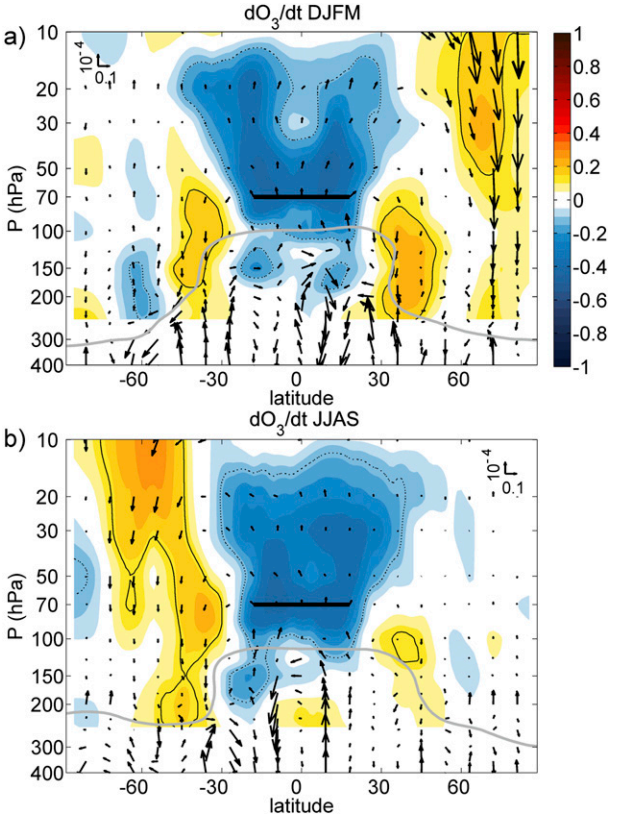

FIG. 4. Regression of the residual circulation (vectors; m s^{-1}) and correlations with zonal mean ozone tendency (colors) from the *Aura* Microwave Limb Sounder (MLS) satellite instrument on tropical upwelling averaged over 18°S–18°N at 70 hPa for (a) DJFM and (b) JJAS for the period 2005–10. The scale of the vectors is indicated for both vertical and horizontal components.

boreal winter (DJFM) and summer (JJAS) seasons are shown in Figs. 5 and 6, respectively. Each figure shows the regressions of the EP flux (Figs. 5a and 6a), zonal wind tendency (Figs. 5b and 6b), and net forcing (Figs. 5c and 6c) onto time series of $\overline{w}^*_m$. The results are qualitatively similar if $\overline{w}^*$ or $\overline{w}^*_Q$ is used instead; however, calculations based on $\overline{w}^*_m$ provide a dynamically consistent estimate.

Regressions onto the global EP flux (Figs. 5a and 6a) show that tropical upwelling in the lower stratosphere is highly correlated with vertical wave propagation and convergence in the extratropical winter stratosphere, primarily over latitudes poleward of 30°. Upwelling is also positively correlated with EP flux divergence in the subtropical upper troposphere (in both hemispheres during DJFM in Fig. 5a, only weakly in the summer hemisphere in JJAS, Fig. 6a), with quasi-horizontal EP flux vectors indicating wave propagation away from these regions. The corresponding regressions onto the zonal mean wind tendencies (Figs. 5b and 6b) show negative correlations (i.e., deceleration of the flow) in the stratosphere centered at the latitude of strongest wave drag in the winter extratropics and positive correlations (acceleration) in the subtropical upper troposphere, approximately mirroring the patterns in EP flux divergence. The extratropical $\overline{u}_t$ patterns extend over a deep layer with an equivalent barotropic vertical structure. There is a global symmetry in the subtropical EP flux and $\overline{u}_t$ patterns in DJFM, which is also evident but less pronounced in JJAS. In the winter hemisphere, the acceleration pattern in the subtropical upper troposphere (linked to subtropical EP flux) extends deeper into the stratosphere, connecting with the (weaker) acceleration induced laterally by the extratropical wave drag (as seen in Fig. 1b). In addition, there is a relatively small region of wind deceleration centered at the equator near the tropopause during DJFM (Fig. 5b), coincident with an EP flux convergence in this region

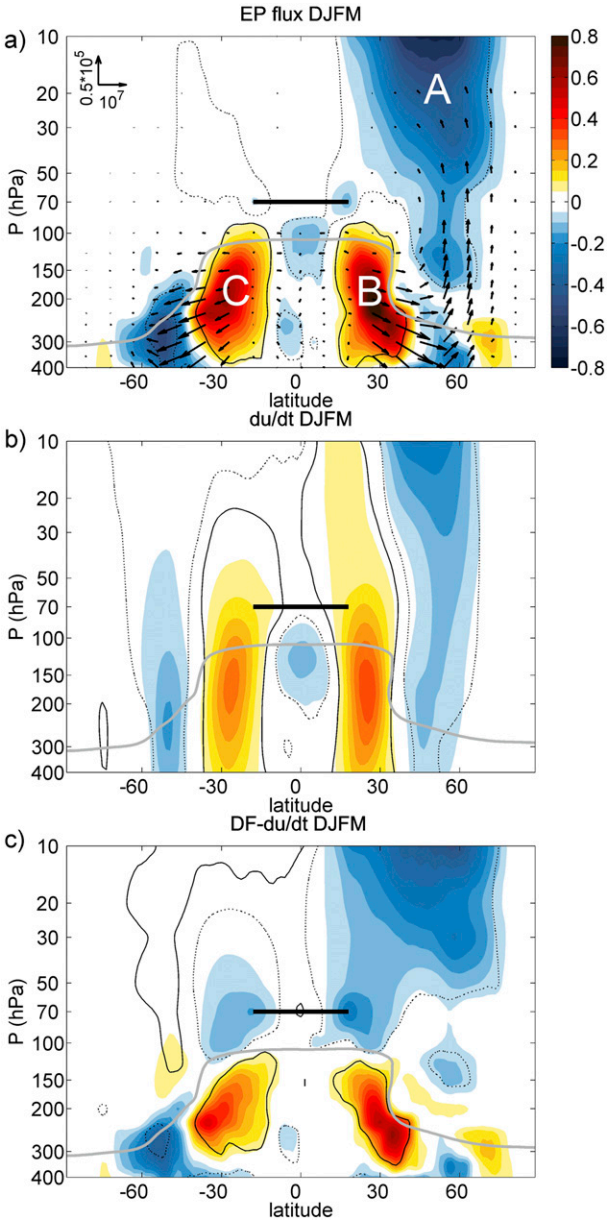

FIG. 5. Regression of (a) EP flux (vectors) and divergence (colors), (b) zonal wind tendency, and (c) net forcing onto upwelling at 70 hPa averaged over 18°S–18°N for DJFM. The scale of the EP flux vectors ($m^3 s^{-2}$) is indicated in (a) for both vertical and horizontal components. The regions A, B, and C in (a) denote centers of action for the EP flux divergence, as discussed in the text. The time series are filtered to remove time scales longer than 90 days. The reference level for upwelling is indicated by the black horizontal bar. The seasonal-mean lapse-rate tropopause is shown in gray. The solid and dashed contours show the threshold of 99% significant linear correlations (positive and negative, respectively). Units for all color-shaded terms are $m s^{-1} day^{-1}$.

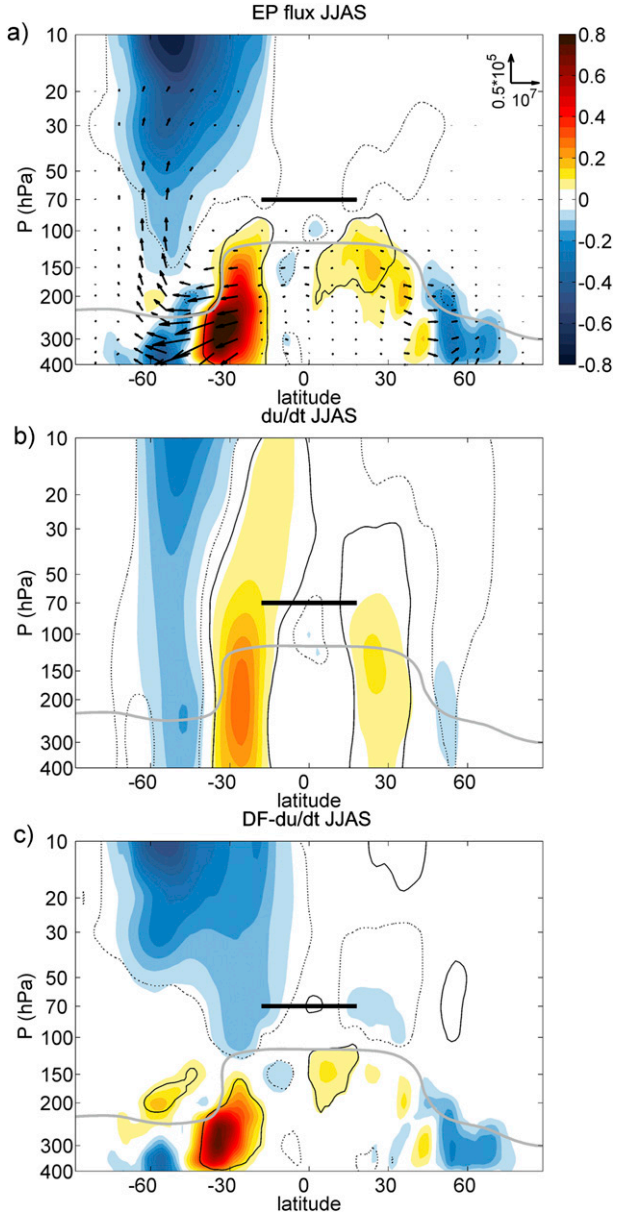

FIG. 6. As in Fig. 5, but for JJAS.

seen in Fig. 5a. Regression patterns for DF $-\overline{u}_t$ (Figs. 5c and 6c) in the winter stratosphere extend laterally farther into the subtropics than those of DF alone and have a maximum near the edges of the tropical upwelling region. The key point is that, while DF may be remote to the tropical lower stratosphere, DF $-\overline{u}_t$ extends into this region where is able to drive upwelling variability [via the balance expressed in Eq. (5)].

The temporal evolution of the regressions during DJFM is shown in Fig. 7, which represents lagged regressions onto $\overline{w}^*_m$ of the fields DF, $\overline{u}_t$, and DF $-\overline{u}_t$, weighted by density and integrated in log-pressure altitude [as they appear in Eq. (5)]. The regression of DF (Fig. 7a) shows strongest values in high latitudes and a systematic propagation of the wave forcing toward low latitudes. The largest values of the projections travel

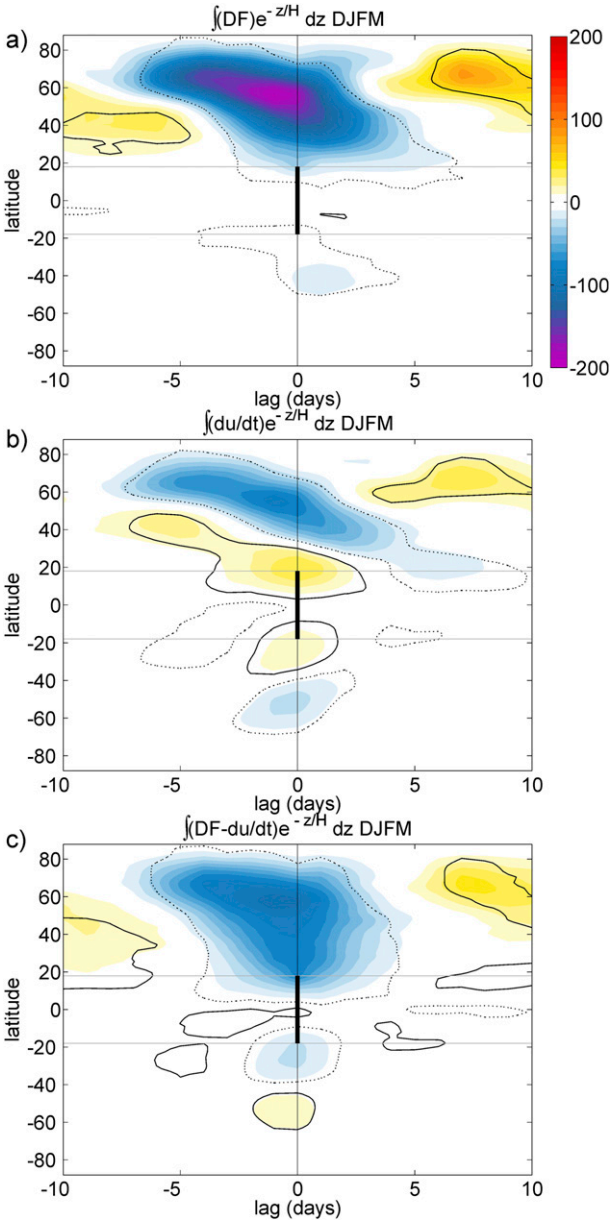

FIG. 7. Lagged regressions as a function of latitude and time (days) of upwelling ($m\,s^{-1}\,day^{-1}$) at 70 hPa averaged over 18°S–18°N with the forcing terms integrated in altitude [as in Eq. (5)] from 70 to 1 hPa for DJFM. The latitudinal boundaries for upwelling calculations (18°S–18°N) are indicated by gray lines. The solid and dashed contours show the threshold of 99% significant linear correlations (positive and negative, respectively).

approximately from 65° to 40°N in about 5 days. This propagation of the transient wave drag from high to low latitudes was recently highlighted by Ueyama et al. (2013). Variations in the corresponding wind tendency (Fig. 7b) show patterns of local deceleration and acceleration that also propagate in a coherent manner toward the tropics. The subtropical acceleration in Fig. 7b is associated with the extratropical (propagating) wave drag and also (around lag 0) with the subtropical upper-troposphere DF (see Figs. 5a,b). The acceleration patterns in the subtropics reach deep into low latitudes, such that $DF - \overline{u}_t$ at low latitudes is substantially stronger than DF alone (Fig. 7c). Figures 5–7 highlight the important role of the zonal wind tendencies induced outside the forcing region for the net forcing of transient tropical upwelling.

b. *Composites of extreme events in tropical upwelling*

The regression patterns in Figs. 3–7 show the statistical signatures of circulations linked to transient tropical upwelling in the lower stratosphere. In this section, these results are complemented with the direct assessment of the EP flux field and its divergence and the zonal mean flow tendency for composited events of extremes in upwelling (both positive and negative). Extreme events composites are constructed based on the multiyear record of $\overline{w}^*_m$ at 70 hPa. Specifically, Fig. 8 shows composites of the EP flux averaged over the 5% of days of strongest and weakest upwelling in boreal winter (DJFM) for the years 1979–2011 as well as the difference (high minus low). Note that the background climatological EP flux is included in the composited fields in Figs. 8a and 8b. Figure 8a shows that the strongest tropical upwelling events are associated with enhanced vertical wave propagation and convergence in the extratropical winter stratosphere, and this behavior is consistent with previous studies (Randel et al. 2002; Ueyama et al. 2013). On the other hand, events of low upwelling (Fig. 8b) are mainly associated with enhanced quasi-horizontal EP flux convergence in the subtropical upper troposphere, with similar patterns observed in both hemispheres, together with weak vertical wave flux in winter high latitudes. Hence, the positive correlations in the subtropical upper troposphere in Fig. 5a imply reduced upwelling associated with enhanced wave drag in these regions. The difference in the EP flux between high and low upwelling extremes (Fig. 8c) produces patterns very similar to the correlations in Fig. 5a (and a structure similar to Fig. 6a is observed for composites during JJAS; not shown).

The corresponding composites for the zonal mean wind tendencies are shown in Fig. 9. Since the climatological mean of the wind tendency is near zero, the anomalies coincide with the absolute values. During maximum upwelling events there is deceleration of the stratospheric winds over roughly 30°–60°N, coincident with the enhanced EP flux convergence in Fig. 8a, and this pattern extends vertically downward across the tropopause. There is also wind acceleration on the equatorward flank of the subtropical jets, extending with

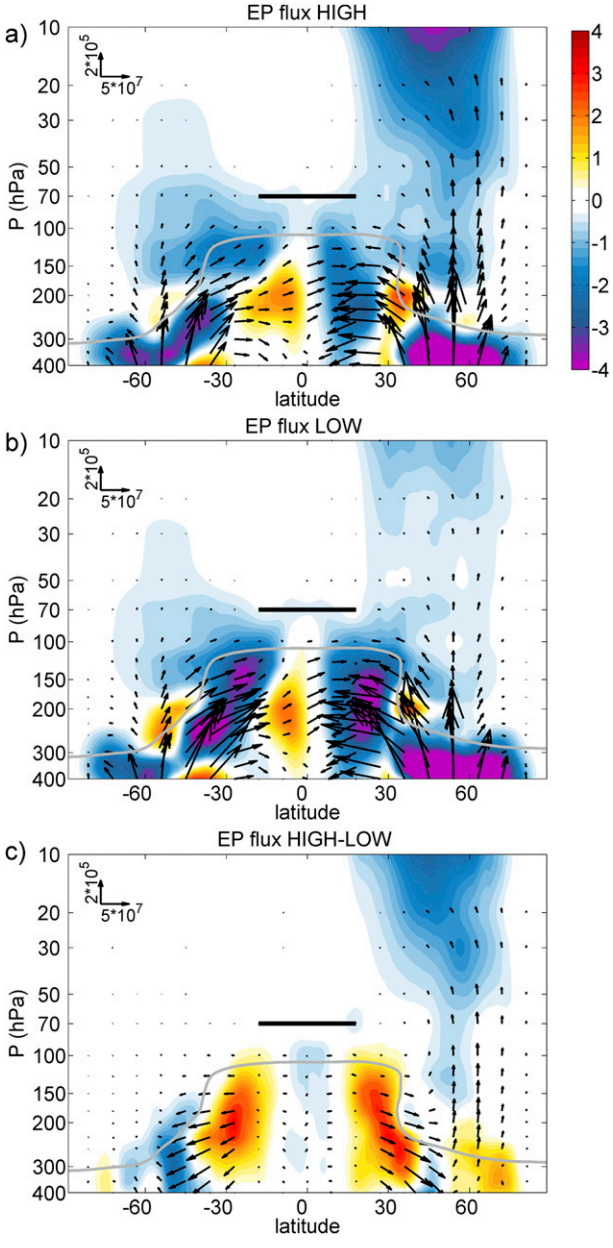

FIG. 8. EP flux (vectors) and divergence (colors) composites for 5% (a) high, (b) low, and (c) difference (high minus low) extremes of upwelling at 70 hPa and averaged over 18°S–18°N for DJFM. The horizontal black bar indicates the location of tropical upwelling used to generate the composites. The seasonal-mean lapse-rate tropopause is shown in gray. The scale of the vectors ($m^3 s^{-2}$) is indicated in the panels for both vertical and horizontal components. Units for all color-shaded terms are $m s^{-1} day^{-1}$.

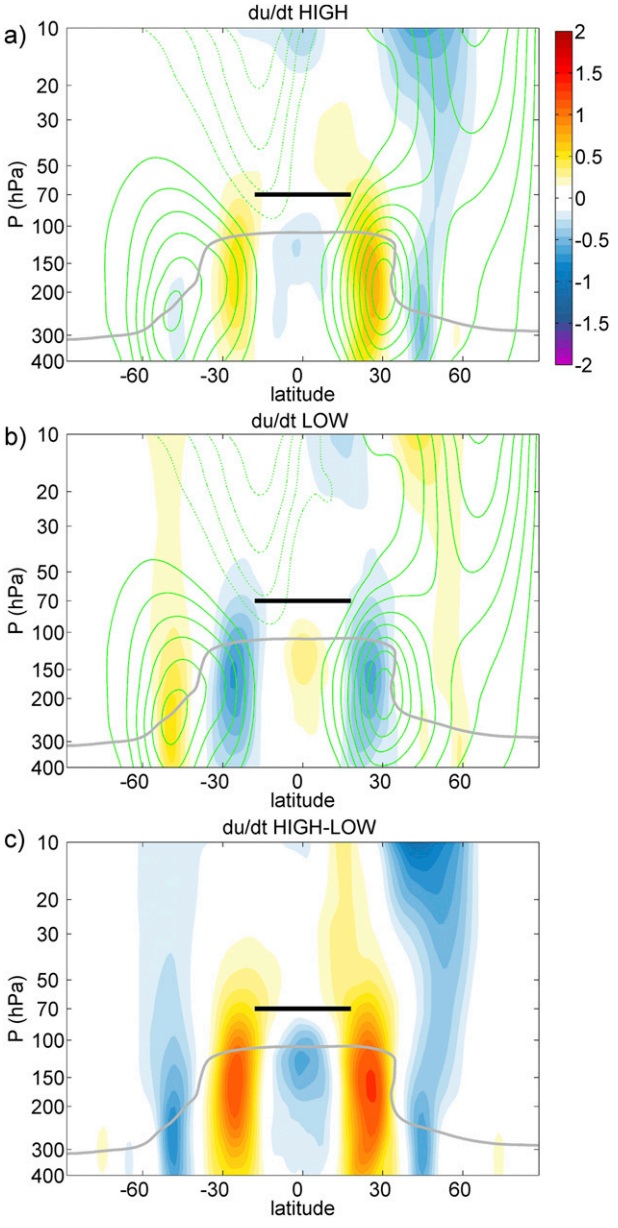

FIG. 9. As in Fig. 8, but for zonal mean wind tendency ($m s^{-1} day^{-1}$). Green contours represent the composited zonal mean winds for the corresponding upwelling extreme events (solid: positive values), with contour interval of $5 m s^{-1}$ (zero contour omitted).

an equivalent barotropic structure over a deep layer from approximately 30 hPa to below 400 hPa. Because the stratospheric EP flux convergence is small at low latitudes, these $\overline{u}_t$ acceleration patterns in the subtropics contribute substantially to the net forcing of $\overline{w}^*_m$ [via Eq. (5)]. The composited $\overline{u}_t$ for the low $\overline{w}^*_m$ extremes (Fig. 9b) show patterns that are approximately mirror images of Fig. 9a, with coherent wind deceleration on the equatorward flanks of the subtropical jets, coinciding with the strong EP flux convergence in Fig. 8b. The zonal wind tendencies extend to higher altitudes across the tropopause, as part of the balanced response including the meridional circulation cell above the forcing (this behavior is clarified in section 3c). The zonal wind tendencies in Figs. 9a and 9b show a symmetric behavior between the two hemispheres, similar to the EP fluxes in Figs. 8a and

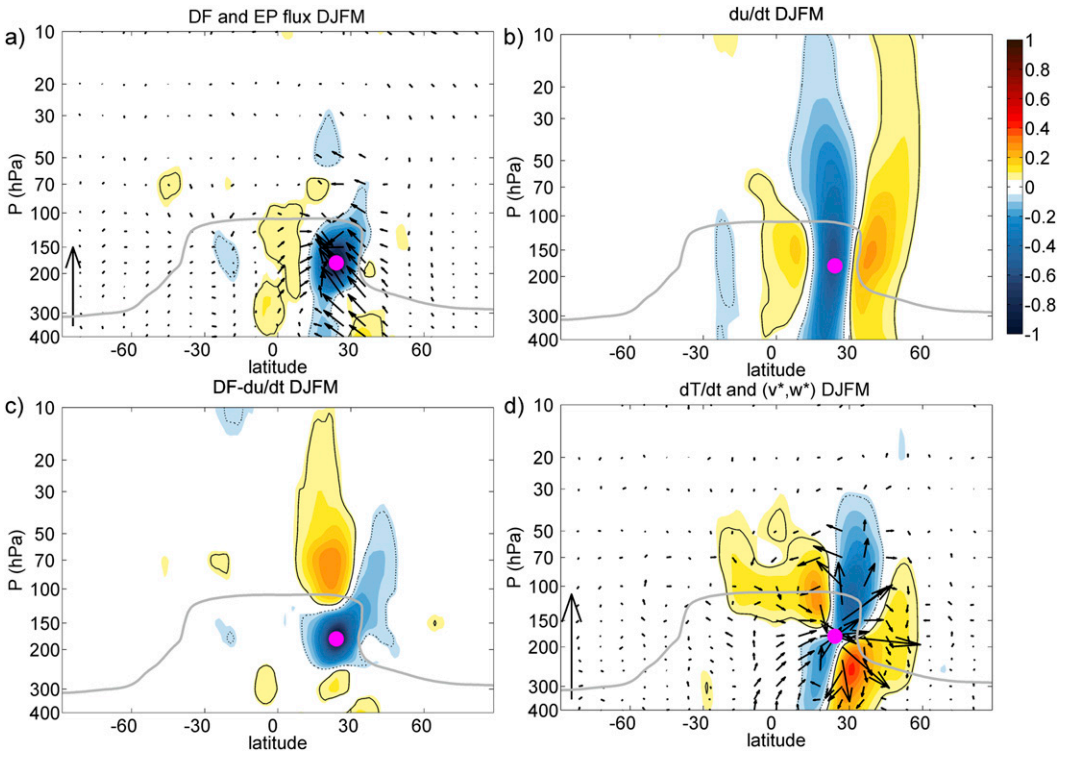

FIG. 10. As in Fig. 1, but one-point correlations of EP flux convergence (−DF) at 24°N, 175 hPa.

8b, but the overall variations in the two hemispheres are uncorrelated, as discussed in section 3d.

c. *Influence of wave forcing in the subtropical upper troposphere*

Calculations of tropical upwelling using Eq. (5) involve integrating the net forcing above the level where upwelling is computed. Hence, it is not evident how the variability in upwelling at 70 hPa is affected by wave drag below that level (i.e., in the subtropical upper troposphere). To appreciate the mechanism through which this influence occurs, Fig. 10 shows one-point correlations of −DF at one point in the subtropical upper troposphere (24°N, 175 hPa) with different fields (as in Fig. 1). In this case, the wave forcing is localized in a relatively narrow vertical and latitudinal region (Fig. 10a), in contrast with the broader forcing region in Fig. 1a. The EP flux vectors suggest a strong contribution to the variability from extratropical waves and additionally some influence from near-equatorial latitudes (i.e., from equatorial planetary waves; Randel et al. 2008). The zonal wind response (Fig. 10b) shows deceleration collocated with the wave drag, extending higher in altitude than the forcing (together with accelerations to the north and south). The different vertical extent of DF and $\overline{u}_t$ results in a dipolar pattern in DF − $\overline{u}_t$, with opposite signs above and below approximately 125 hPa (Fig. 10c). Consequently, from the point of view of the upwelling diagnostic via Eq. (5), the remote influence of the upper-tropospheric wave forcing on upwelling near and above the tropical tropopause occurs through the deep response of the zonal wind. Dynamically, such wind response is associated with the meridional circulation and corresponding changes in temperature induced by the forcing, shown in Fig. 10d. As expected from theory, two circulation cells are observed above and below the forcing, together with a quadrupole temperature structure. The circulation cell above the forcing includes downwelling and warming near the tropical tropopause (extending across the equator and into the SH subtropics) as well as cooling in the upwelling region approximately over 25°–40°N. This is the structure observed in meridional circulation and temperature correlations linked to upwelling near the tropopause (e.g., Fig. 3), and is the statistical signature of the shallow branch of the BDC, as will be further shown in section 3e.

d. *Relations of wave forcing between high and low latitudes and between hemispheres*

The results of $\overline{w}^*_m$ regressions (Figs. 5 and 6) and extreme upwelling events (Figs. 8 and 9) demonstrate the combined influence of wave forcing in the winter high-latitude stratosphere and subtropical upper troposphere (regions A and B in Fig. 5a), and also show symmetric

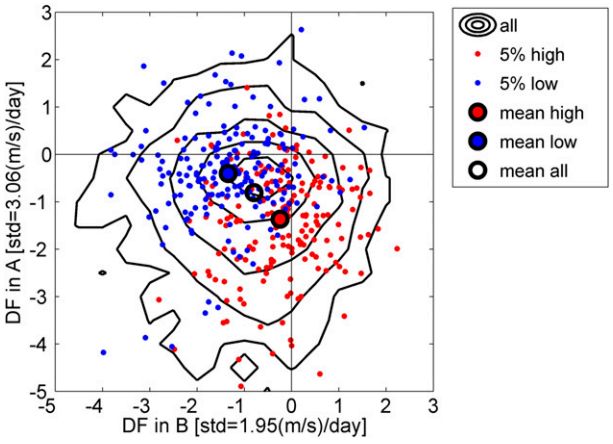

FIG. 11. Two-dimensional distribution of wave forcing in the extratropical winter stratosphere (average over 20–10 hPa and 36°–60°N; region A in Fig. 5a) vs wave forcing in the subtropical upper troposphere (average over 300–125 hPa and 21°–33°N; region B in Fig. 5a) for DJFM. The axes are normalized to standard deviations in each quantity. Black contours show probability distribution of all DJFM days during 1979/80–2010/11 (contours shown are 1%, 5%, 20%, 50%, and 80%). Red and blue dots show days with 5% extreme maximum and minimum tropical upwelling. Larger circles indicate the mean of the distribution of all points (white), high extremes (red), and low extremes (blue).

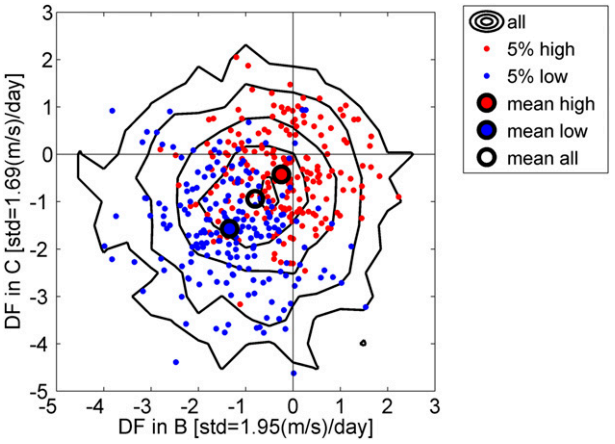

FIG. 12. As in Fig. 11, but for wave forcing in the subtropical upper troposphere in the NH vs the SH (averages over 300–125 hPa and 21°–33°N and 21°–33°S, respectively; regions B and C in Fig. 5a).

patterns between the subtropics in both hemispheres (regions B and C in Fig. 5a; this latter behavior is stronger in DJFM than in JJAS). In this section we examine whether these patterns represent systematic connections between these forcing regions.

First, the links between high- and low-latitude wave forcing are examined. Figure 11 shows a two-dimensional histogram of DF in the extratropical stratosphere (average over 36°–60°N, 20–10 hPa; region A; Fig 11a) and the subtropical upper troposphere (21°–33°N, 300–125 hPa; region B; Fig 11b). The black contours in Fig. 11 illustrate the distribution of all daily DJFM samples during 1979/80–2010/11 ($121\ \text{days yr}^{-1} \times 32\ \text{yr} = 3872$ days), and the overall circular pattern of contours is evidence of weak correlation of wave forcing between regions A and B (i.e., enhanced wave drag in region A is not necessarily associated with reduced wave drag in region B). This is consistent with the direct calculation of time series correlation, which is statistically insignificant (~0.03). Figure 11 further includes red and blue dots indicating days with positive and negative extremes in $\overline{w}^*_m$ (the top and bottom 5%, as in the composite events described above). These extreme cases are systematically skewed compared to the background distribution, so that enhanced tropical upwelling corresponds to stronger negative high-latitude DF (Fig 11a) and weaker negative (or positive) subtropical DF (Fig 11b). Weak extremes in tropical upwelling correspond to the opposite behavior: stronger subtropical DF and weaker negative or positive high-latitude DF. These are the patterns identified in Fig. 8, and the differences in the forcing between strong and weak upwelling extremes are statistically significant. Figure 11 proves that the time series of wave forcing in high and low latitudes are generally uncorrelated, and events where these effects reinforce lead to extremes in $\overline{w}^*_m$ (such that the patterns in composited events appear linked between high and low latitudes). Similar conclusions are obtained when comparing EP fluxes (i.e., high-latitude $\overline{v'T'}$ and subtropical $\overline{u'v'}$) instead of DF.

Figure 12 shows a similar diagnostic comparing wave forcing in the subtropics of each hemisphere—that is, DF averaged over 300–125 hPa for 21°–33°N (region B) and for 21°–33°S (region C). Again the overall two-dimensional distribution suggests little correlation between wave forcing in each hemisphere (as also inferred from Fig. 10a). Positive extreme tropical upwelling events (red dots in Fig. 12) occur when DF is less negative or positive in both hemispheres, and the opposite extremes occur when DF is more negative in both hemispheres. While there is no general correlation between hemispheres, events that occur simultaneously lead to tropical upwelling extremes and appear as symmetric patterns in statistical correlations. Equivalent conclusions are found when comparing $\overline{u}_t$ links between hemispheres. We note that, although Figs. 8, 9, 11, and 12 are based on the 5% extreme events, the described relations do not depend on the fraction of extreme events considered and thus these results are representative of the general behavior (not shown).

e. *Shallow and deep branches of the residual circulation*

Analyses of circulation statistics and tracer behavior suggest that the stratospheric Brewer–Dobson circulation

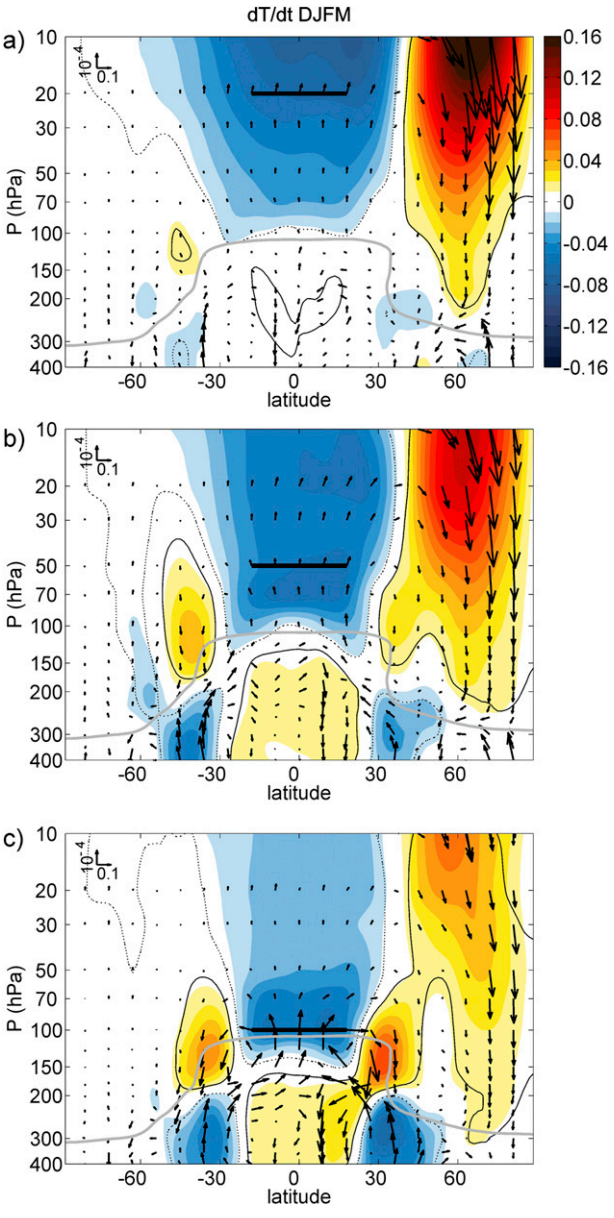

FIG. 13. As in Fig. 3a, but for tropical upwelling computed at (a) 20, (b) 50, and (c) 100 hPa, as indicated by the black bars.

can be described by deep and shallow branches, which can evolve in different ways (e.g., Plumb 2002; Birner and Bönisch 2011). This characteristic is also found in the analyses of subseasonal variability in this work (see Figs. 3 and 4). Figure 13 illustrates the transition from shallow to deep residual circulation in ERA-Interim data derived by regressing global circulation onto the tropical upwelling at different altitudes. The statistical signature of the lower branch can be identified in correlations with $\overline{w}^*_m$ at 100 hPa (Fig. 13c) as shallow circulation cells centered near the altitude of the tropical tropopause, with downwelling and warming patterns near 25°–40°N and 25°–40°S. In contrast, correlations with $\overline{w}^*_m$ at higher altitudes show less evidence of this feature, and it is nearly absent from correlations with $\overline{w}^*_m$ at 20 hPa. The 20-hPa correlations reflect primarily the upper branch of the BDC, with broad tropical upwelling and downwelling in the winter polar stratosphere (Fig. 13a). The change between the low and high branches of the residual circulation appears in Fig. 13 as a smooth transition between 1) shallow overturning, with downwelling and warming in the subtropics, and 2) deep upwelling, broad cooling of the tropical lower and middle stratosphere, and warming at high winter latitudes. Tropical upwelling in the region near 70–50 hPa is correlated with both branches. Note that upwelling at 100 hPa still appears connected with the deep branch, as shown by the significant correlations with downwelling and warming at high latitudes.

The transition of the residual circulation from the lower to the middle stratosphere is also reflected in distinctive patterns of forcing terms influencing upwelling at different levels. Figure 14 shows the regression of the EP flux onto upwelling at the different levels, showing a transition in the dominant forcing associated with upwelling variability at different levels. Near 20 hPa, upwelling is most affected by forcing in the winter extratropical stratosphere (Fig. 14a), while the lower branch of the BDC is most influenced by transient wave forcing in the subtropical upper troposphere and lower stratosphere (Fig. 14c). Note that the shallow circulation (Fig. 14c) is negatively correlated with DF in the subtropical lower stratosphere near and above the level of upwelling, while positive correlations are found just below (as discussed in section 3c). This behavior is consistent with the results of Grise and Thompson (2013), as will be further discussed in the next section. Finally, note that extratropical wave drag is also correlated with upwelling at 100 hPa, which could be linked to the connection with the deep branch seen in Fig. 13c.

4. Summary and discussion

Upwelling across the tropical tropopause is a fundamental part of the global stratospheric circulation. It cannot be observed directly but can be inferred from thermodynamic or momentum calculations, or obtained from meteorological reanalyses, and these three estimates agree well for levels in the lower stratosphere (Abalos et al. 2012). Tropical upwelling is primarily driven by dynamical forcing (with temperatures and radiative balances responding to this forcing), which is embedded within the calculations of upwelling based on momentum balance $\overline{w}^*_m$. This work focuses on examining the dynamical drivers of $\overline{w}^*_m$ by quantifying

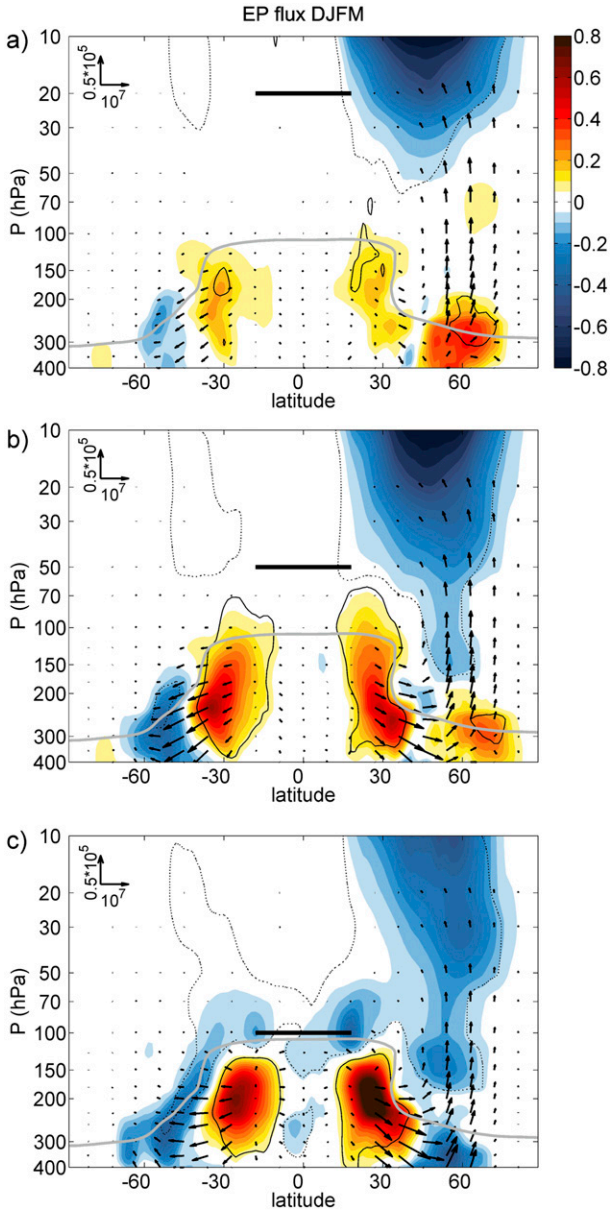

FIG. 14. As in Fig. 5a, but for tropical upwelling computed at (a) 20, (b) 50, and (c) 100 hPa, as indicated by the black bars.

relationships with the forcing DF and its effect on the zonal wind tendency $\overline{u}_t$, both directly linked to $\overline{w}^*_m$ via Eq. (5). Derived estimates of upwelling in the lower stratosphere exhibit an important component of subseasonal (week to week) variability in addition to a large annual cycle (Fig. 2). Mechanisms contributing to driving the annual cycle include forcing from extratropical waves (Yulaeva et al. 1994; Ueyama and Wallace 2010), baroclinic waves dissipating in the subtropics (Taguchi 2009; Chen and Sun 2011), and equatorial planetary waves (Boehm and Lee 2003; Kerr-Munslow and Norton 2006; Randel et al. 2008; Ortland and Alexander 2014), although causal mechanisms are still a topic of active research (note that the forcings of the annual cycle are difficult to isolate based simply on correlations). In contrast, the subseasonal variations in upwelling (e.g., Fig. 2) have a distinctive temporal signature that can be used to identify transient forcing mechanisms, and this is the goal of this study.

Regression analysis and composites of extreme tropical upwelling ($\overline{w}^*_m$) events, based on ERA-Interim data for 1979–2011, highlight two key regions of wave forcing for lower-stratospheric upwelling: namely, the extratropical winter stratosphere and the subtropical upper troposphere (regions A and B/C in Fig. 5a). Enhanced tropical upwelling in the lower stratosphere (70 hPa) occurs in conjunction with stronger high-latitude stratospheric wave forcing (enhanced upward EP flux, proportional to $\overline{v'T'}$) and reduced wave forcing in the subtropical upper troposphere (weaker meridional EP flux, proportional to $\overline{u'v'}$). Weaker tropical upwelling occurs with reduced high-latitude $\overline{v'T'}$ and enhanced subtropical $\overline{u'v'}$. These represent modulations of the time-mean climatological EP flux and divergence in the extratropics (Fig. 8).

The nonlocal response to transient localized wave drag (DF) consists of two meridional circulation cells of opposite sense: one above and one below the forcing (the lower mass circulation cell is stronger because of the higher density). These extend outside the horizontal scale of the forcing and are linked to tendencies of zonal wind $\overline{u}_t$ and temperature $\overline{T}_t$ acting to maintain thermal wind balance (e.g., Garcia 1987; Haynes et al. 1991). In this work, the statistical signature of this coupled response is examined in reanalysis data for the identified forcing regions relevant for transient upwelling [the extratropical stratosphere (Fig. 1) and the subtropical upper troposphere (Fig. 10)]. Although the meridional circulation and $\overline{u}_t$ are closely coupled aspects of the response to the time-dependent forcing (DF), from the diagnostic perspective of Eq. (5) the term $\mathrm{DF} - \overline{u}_t$ can be regarded as the net forcing of upwelling, as it constitutes the combined momentum forcing in the $\overline{w}^*_m$ calculation. In this sense, the net forcing associated with the extratropical forcing (DF) in Fig. 1 extends into tropical latitudes, where it impacts upwelling variability [Eq. (5)]. Equivalently, the effect of the localized forcing in the subtropical upper troposphere on $\overline{u}_t$ extends vertically across the tropopause in Fig. 10, resulting in relative downwelling over the tropical tropopause.

The regression and composited patterns of DF based on $\overline{w}^*_m$ at 70 hPa (Figs. 5a and 8) suggest the combined influence of high- and low-latitude wave forcing on tropical upwelling and also show highly symmetric

patterns of subtropical wave forcing in each hemisphere (at least during DJFM). This begs the question of whether the wave forcings in these regions are intrinsically linked or if this is a result of studying correlated variations with $\overline{w}^*_m$. This question has been addressed by examining cross correlations and the two-dimensional distribution of forcing between the different regions. The results (Figs. 11 and 12) show that, while the three forcing regions (A, B, and C) are linked to tropical upwelling, the variability of the wave forcing itself in these regions is not systematically correlated. Rather, extreme upwelling events (both positive and negative) occur when the variations in wave driving in the different regions happen to reinforce each other; for example, occasional coincident events of enhanced subtropical wave forcing in both hemispheres leads to reduced tropical upwelling (Figs. 8b and 12). Our conclusion is that the coherent global variations suggested in regressions and extreme composites do not signify distant, globally coherent behavior in wave forcing.

The statistical relationships between derived tropical upwelling in the lower stratosphere and global temperature and circulation reveal the shallow and deep branches of the Brewer–Dobson circulation (e.g., Fig. 3). The upper branch of the BDC is most strongly correlated to tropical upwelling at levels above the lower stratosphere, highlighting a broad-scale deep circulation connecting the tropics and the winter polar stratosphere (Fig. 13a). Variability in the deep branch is primarily linked to wave forcing in the high-latitude winter stratosphere (Fig. 14a). In contrast, transient upwelling near the tropopause (~100 or 70 hPa) is strongly correlated with downwelling circulation cells near the tropopause level in the subtropics (~25°–40°N/S), and these are reflected in zonal average temperature (Fig. 13c) and ozone tendencies (Fig. 4). This behavior is primarily linked to variability in wave forcing in the subtropical upper troposphere (Fig. 14c), wherein stronger (weaker)-than-average wave forcing affects the overturning circulation cells above the forcing, leading to reduced (enhanced) upwelling over the tropical tropopause and corresponding sinking in the subtropics (Fig. 10d). Note that the shallow branch of the BDC is also intensified by stronger convergence in the subtropical lower stratosphere (Fig. 14c). Hence, the exact altitude at which wave dissipation occurs in the subtropics is crucial for the variability of the shallow branch of the BDC, as the drag at slightly different levels can have opposite effects on upwelling near the tropopause. These results are consistent with the calculations of Grise and Thompson (2013), inferred from high-vertical-resolution GPS temperature observations. They show that wave drag in the subtropical lower stratosphere is associated with cooling near the tropical tropopause (~100–70 hPa), while subtropical tropospheric forcing leads to warming. Our analyses demonstrate the dynamical mechanism underlying these relationships, in terms of the momentum balance equation. Specifically, as follows from Eq. (5), subtropical EP flux convergence between 100 and 70 hPa drives stronger upwelling near the tropopause, while the wave drag at lower levels weakens the upwelling through the induced remote response in the zonal wind, as illustrated in Fig. 10.

The statistical analyses in the present work suggest an overall smooth transition between the two branches of the BDC, with upwelling at 100 hPa not fully decoupled from the deep circulation and the shallow branch reaching up to about 50 hPa (Fig. 13), consistently with the picture provided by the trajectory analysis of Birner and Bönisch (2011). Our results, based on time series of tropical upwelling, are also in general agreement with those obtained by Ueyama et al. (2013), based on temperature tendencies, which highlight distinct variability in circulation (and links to high-latitude wave forcing) in the tropics between 100 and 70 hPa and above. However, the latter work suggests a more abrupt disconnection between the shallow and the deep branches of the Brewer Dobson circulation than our results.

Acknowledgments. We thank Cameron Homeyer for facilitating access to ERA-Interim data used here. We are very grateful to Thomas Birner, Rolando Garcia, Rei Ueyama, Mike Wallace, and two anonymous referees for comments and suggestions, which have significantly improved the paper. This work was partially supported under the NASA Aura Science Program. M.A. also acknowledges the Spanish projects CGL2008-06295 and CGL2012-34997 and NCAR for hosting her visits.

REFERENCES

Abalos, M., W. J. Randel, and E. Serrano, 2012: Variability in upwelling across the tropical tropopause and correlations with tracers in the lower stratosphere. *Atmos. Chem. Phys.,* **12,** 11 505–11 517, doi:10.5194/acp-12-11505-2012.

——, ——, D. E. Kinnison, and E. Serrano, 2013: Quantifying tracer transport in the tropical lower stratosphere using WACCM. *Atmos. Chem. Phys.,* **13,** 10 591–10 607, doi:10.5194/acp-13-10591-2013.

Andrews, D. G., J. R. Holton, and C. B. Leovy, 1987: *Middle Atmosphere Dynamics.* International Geophysics Series, Vol. 40, Academic Press, 489 pp.

Birner, T., and H. Bönisch, 2011: Residual circulation trajectories and transit times into the extratropical lowermost stratosphere. *Atmos. Chem. Phys.,* **11,** 817–827, doi:10.5194/acp-11-817-2011.

Boehm, M. T., and S. Lee, 2003: The implications of tropical Rossby waves for tropical tropopause cirrus formation and for the equatorial upwelling of the Brewer–Dobson circulation. *J. Atmos. Sci.,* **60,** 247–261, doi:10.1175/1520-0469(2003)060<0247:TIOTRW>2.0.CO;2.

Butchart, N., and Coauthors, 2006: Simulations of anthropogenic change in the strength of the Brewer–Dobson circulation. *Climate Dyn.,* **27,** 727–741, doi:10.1007/s00382-006-0162-4.

Calvo, N., and R. R. Garcia, 2009: Wave forcing of the tropical upwelling in the lower stratosphere under increasing concentrations of greenhouse gases. *J. Atmos. Sci.,* **66,** 3184–3196, doi:10.1175/2009JAS3085.1.

Chen, G., and L. Sun, 2011: Mechanisms of the tropical upwelling branch of the Brewer–Dobson circulation: The role of extratropical waves. *J. Atmos. Sci.,* **68,** 2878–2892, doi:10.1175/JAS-D-11-044.1.

Dee, D. P., and Coauthors, 2011: The ERA-Interim reanalysis: Configuration and performance of the data assimilation system. *Quart. J. Roy. Meteor. Soc.,* **137,** 553–597, doi:10.1002/qj.828.

Dunkerton, T. J., C.-P. F. Hsu, and M. E. McIntyre, 1981: Some Eulerian and Lagrangian diagnostics for a model stratospheric warming. *J. Atmos. Sci.,* **38,** 819–843, doi:10.1175/1520-0469(1981)038<0819:SEALDF>2.0.CO;2.

Fritz, S., and S. D. Soules, 1972: Planetary variations of stratospheric temperatures. *Mon. Wea. Rev.,* **100,** 582–589, doi:10.1175/1520-0493(1972)100<0582:PVOST>2.3.CO;2.

Garcia, R. R., 1987: On the mean meridional circulation of the middle atmosphere. *J. Atmos. Sci.,* **44,** 3599–3609, doi:10.1175/1520-0469(1987)044<3599:OTMMCO>2.0.CO;2.

——, and W. J. Randel, 2008: Acceleration of the Brewer–Dobson circulation due to increases in greenhouse gases. *J. Atmos. Sci.,* **65,** 2731–2739, doi:10.1175/2008JAS2712.1.

Garny, H., M. Dameris, W. J. Randel, G. E. Bodeker, and R. Deckert, 2011: Dynamically forced increase of tropical upwelling in the lower stratosphere. *J. Atmos. Sci.,* **68,** 1214–1233, doi:10.1175/2011JAS3701.1.

Grise, K. M., and D. J. Thompson, 2013: On the signatures of equatorial and extratropical wave forcing in tropical tropopause layer temperatures. *J. Atmos. Sci.,* **70,** 1084–1102, doi:10.1175/JAS-D-12-0163.1.

Haynes, P. H., C. J. Marks, M. E. McIntyre, T. G. Shepherd, and K. P. Shine, 1991: On the ''downward control'' of extratropical diabatic circulations by eddy-induced mean zonal forces. *J. Atmos. Sci.,* **48,** 651–678, doi:10.1175/1520-0469(1991)048<0651:OTCOED>2.0.CO;2.

Holton, J. R., P. H. Haynes, M. E. McIntyre, A. R. Douglass, R. B. Rood, and L. Pfister, 1995: Stratosphere–troposphere exchange. *Rev. Geophys.,* **33,** 403–439, doi:10.1029/95RG02097.

Kerr-Munslow, A. M., and W. A. Norton, 2006: Tropical wave driving of the annual cycle in tropical tropopause temperatures. Part I: ECMWF analyses. *J. Atmos. Sci.,* **63,** 1410–1419, doi:10.1175/JAS3697.1.

North, G. R., T. L. Bell, R. F. Cahalan, and F. J. Mohen, 1982: Sampling errors in the estimation of empirical orthogonal functions. *Mon. Wea. Rev.,* **110,** 699–706, doi:10.1175/1520-0493(1982)110<0699:SEITEO>2.0.CO;2.

Ortland, D. A., and M. J. Alexander, 2014: The residual-mean circulation in the tropical tropopause layer driven by tropical waves. *J. Atmos. Sci.,* **71,** 1305–1322, doi:10.1175/JAS-D-13-0100.1.

Plumb, R. A., 2002: Stratospheric transport. *J. Meteor. Soc. Japan,* **80,** 793–809, doi:10.2151/jmsj.80.793.

——, and J. Eluszkiewicz, 1999: The Brewer–Dobson circulation: Dynamics of the tropical upwelling. *J. Atmos. Sci.,* **56,** 868–890, doi:10.1175/1520-0469(1999)056<0868:TBDCDO>2.0.CO;2.

Randel, W. J., 1993: Global variations of zonal mean ozone during stratospheric warming events. *J. Atmos. Sci.,* **50,** 3308–3321, doi:10.1175/1520-0469(1993)050<3308:GVOZMO>2.0.CO;2.

——, R. R. Garcia, and F. Wu, 2002: Time-dependent upwelling in the tropical lower stratosphere estimated from the zonal-mean momentum budget. *J. Atmos. Sci.,* **59,** 2141–2152, doi:10.1175/1520-0469(2002)059<2141:TDUITT>2.0.CO;2.

——, M. Park, F. Wu, and N. Livesey, 2007: A large annual cycle in ozone above the tropical tropopause linked to the Brewer–Dobson circulation. *J. Atmos. Sci.,* **64,** 4479–4488, doi:10.1175/2007JAS2409.1.

——, R. R. Garcia, and F. Wu, 2008: Dynamical balances and tropical stratospheric upwelling. *J. Atmos. Sci.,* **65,** 3584–3595, doi:10.1175/2008JAS2756.1.

Ryu, J.-H., and S. Lee, 2010: Effect of tropical waves on the tropical tropopause transition layer upwelling. *J. Atmos. Sci.,* **67,** 3130–3148, doi:10.1175/2010JAS3434.1.

Semeniuk, K., and T. G. Shepherd, 2001: Mechanisms for tropical upwelling in the stratosphere. *J. Atmos. Sci.,* **58,** 3097–3115, doi:10.1175/1520-0469(2001)058<3097:MFTUIT>2.0.CO;2.

Shepherd, T. G., 2007: Transport in the middle atmosphere. *J. Meteor. Soc. Japan,* **85,** 165–191, doi:10.2151/jmsj.85B.165.

——, and C. McLandress, 2011: A robust mechanism for strengthening of the Brewer–Dobson circulation in response to climate change: Critical-layer control of subtropical wave breaking. *J. Atmos. Sci.,* **68,** 784–797, doi:10.1175/2010JAS3608.1.

Taguchi, M., 2009: Wave driving in the tropical lower stratosphere as simulated by WACCM. Part I: Annual cycle. *J. Atmos. Sci.,* **66,** 2029–2043, doi:10.1175/2009JAS2854.1.

Ueyama, R., and J. M. Wallace, 2010: To what extent does high-latitude wave forcing drive tropical upwelling in the Brewer–Dobson circulation? *J. Atmos. Sci.,* **67,** 1232–1246, doi:10.1175/2009JAS3216.1.

——, E. P. Gerber, J. M. Wallace, and D. M. W. Frierson, 2013: The role of high-latitude waves in the intraseasonal to seasonal variability of tropical upwelling in the Brewer–Dobson circulation. *J. Atmos. Sci.,* **70,** 1631–1648, doi:10.1175/JAS-D-12-0174.1.

Yulaeva, E., J. R. Holton, and J. M. Wallace, 1994: On the cause of the annual cycle in tropical lower-stratospheric temperature. *J. Atmos. Sci.,* **51,** 169–174, doi:10.1175/1520-0469(1994)051<0169:OTCOTA>2.0.CO;2.

Zhou, T., M. A. Geller, and W. Lin, 2012: An observational study on the latitudes where wave forcing drives Brewer–Dobson upwelling. *J. Atmos. Sci.,* **69,** 1916–1935, doi:10.1175/JAS-D-11-0197.1.